Combined effect of Stark and singlet-triplet mixing on photon-yield spectra of singly excited helium

A. Mihelič,[1] M. Žitnik,[1,2] K. C. Prince,[3,4] M. Coreno,[5] and R. Richter[3]
[1]*Jožef Stefan Institute, Jamova cesta 39, SI-1000 Ljubljana, Slovenia*
[2]*Faculty of Mathematics and Physics, Jadranska ulica 19, SI-1000 Ljubljana, Slovenia*
[3]*Sincrotrone Trieste, AREA Science Park, I-34149 Basovizza (Trieste), Italy*
[4]*CNR-IOM, AREA Science Park, I-34149 Basovizza (Trieste), Italy*
[5]*CNR-IMIP, Montelibretti, I-00016 Roma, Italy*
(Received 27 September 2011; published 22 February 2012)

We present a theoretical framework for the calculation of photon-yield spectra from radiative-cascade decays of photoexcited helium atoms in a static electric field for incident photon energies below the first ($N = 1$) ionization threshold. The present theory takes full account of the singlet-triplet mixing among the singly excited states with principal quantum numbers $n \lesssim 10$. The model predicts the enhancement of transition probabilities to triplet final states due to the field-induced mixing. In particular, for a field strength of 9.17 kV/cm, polarization of incident photons perpendicular to the field, and a 4 meV broad excitation function tuned to the $1s6p\,^1P$ states, the $1s6\ell \rightarrow 1s2p\,^3P$ and $1s5\ell \rightarrow 1s2p\,^3P$ emitted photon yields are predicted to be about 70 times and 20 times lower, respectively, than the photon yields for transitions to the corresponding singlet final states.

DOI: 10.1103/PhysRevA.85.023421 PACS number(s): 32.60.+i, 31.15.aj, 32.50.+d

I. INTRODUCTION

Noble-gas atomic targets, and helium in particular, are suitable for testing novel experimental, theoretical, and computational techniques dealing with photon and electron beams. The advantage of the former is the constraint of the strict selection rules, which may simplify the theoretical treatment and interpretation of experimental data. At the same time, these rules impose a limit on reaching states with higher angular momenta or the forbidden-parity states. When considered as a deficiency, such a situation can be circumvented by more or less efficient preparation of target states with different symmetries [1] or by multiphoton excitation. For example, a combination of a synchrotron pump and an infrared laser probe resulted in excellent energy resolution, by means of which the states close to ionization thresholds could be examined [2], and even-parity doubly excited states of helium were studied with two-photon excitation with intense free-electron-laser pulses [3].

Another way of accessing dipole-forbidden states is by external electric or magnetic fields. These states can be reached indirectly by field-induced mixing with the optically accessible states. The fluorescence spectra emitted by Stark-split manifolds of singly excited helium states in the discharge tube were reported already in the 1920s (e.g., Refs. [4,5]), and confirmed the validity of Schrödinger's quantum-mechanical treatment [6]. Later on, the gross features of the fluorescence spectra emitted from singly excited helium were considered well understood and served mostly for field-strength calibration purposes (Ref. [7] and the references therein).

The motivation for the present studies comes from a recent experiment where photon-induced spin-flip transitions in helium were measured by observation of triplet metastable atom yields [8]. The ground-state helium atoms were photoexcited to doubly excited states below the $N = 2$ ionization threshold. The most likely radiative transitions for these states are to singly excited states, which, in turn, decay to the ground state or to long-lived singlet and triplet metastable states by radiative cascades. The singlet-triplet crossover, which occurs either between the doubly excited states or between the singly excited states, was investigated with a helium quenching lamp. To differentiate between the atoms which end in the singlet and the triplet metastable states, the lamp was used to reduce the number of atoms in the singlet metastable state by inducing the singlet $1s2s \rightarrow 1s2p$ transitions and exploiting the fact that the $1s2p$ singlet states decay mostly to the ground state. By comparison of the total (singlet + triplet) metastable-atom-yield spectra with the light switched on and off, information on the population of the triplet metastable states could be extracted. This experiment indicated that a considerable part of the triplet metastable yield may be a consequence of the singlet-triplet mixing between the singly excited states, as opposed to the mixing between the doubly excited states that was first believed to be the main mechanism for generation of the triplet metastable atoms.

To shed some light on that problem, we have undertaken an accurate modeling of the radiative cascades of the singly excited states which follow the photoexcitation of the ground-state helium atoms in the presence of a static electric field. We are concerned with the effect of the field-induced angular momenta mixing between the singly excited states with moderate principal quantum numbers if the singlet-triplet mixing between these states is fully taken into account. It is rather interesting to study the combined effect: while the electric field in first order couples quantum states with different angular momenta and parity but with the same total spin, the singlet-triplet mixing occurs between the states with equal parity and equal total angular momenta. Furthermore, the coupling between the singlet and triplet states is strongest for states with the same principal quantum numbers and equal *orbital* angular momenta [9]. The singlet-triplet mixing between the singly excited states is practically negligible for states with low orbital angular momenta and almost complete for states with higher orbital angular momenta. It may therefore be expected that, under specific conditions, the presence of an external field could modify the photon yield associated with transitions to predominantly triplet states.

Specifically, we present the calculated photon yields for the cascade decay of $n = 6$ states which end in the low-lying $1s2p$ singlet and triplet states. Our theoretical predictions suggest that (i) the photon yields for transitions ending in the triplet states are extremely sensitive to the effect of the singlet-triplet mixing in the presence of the electric field, and (ii) it may be possible to detect some of these transitions in future experiments to validate the model.

II. DESCRIPTION OF THE PROBLEM

In the present work, we concentrate on radiative-decay cascades which follow photoexcitation of the ground-state atoms to the states of the $n = 6$ manifold in an external field. These cascades—which consist of an absorption step and $\mathfrak{n} = 1,2,\ldots$ emission steps—can be described with the following symbolically written reaction (Fig. 1):

$$1s^2 \xrightarrow[\text{(a)}]{\hbar\omega_0} 1s6\ell \xrightarrow[\text{(e)}]{\hbar\omega_1} 1sn'\ell' \xrightarrow[\text{(e)}]{\hbar\omega_2} \cdots \xrightarrow[\text{(e)}]{\hbar\omega_{\mathfrak{n}}} 1sn_f\ell_f, \qquad (1)$$

where (a) stands for photon absorption and (e) for photon emission. Note that the total angular momentum is no longer preserved in the external field, so that the configuration labels used in Eq. (1) signify the zero-field states mixed by the field. It has been taken into account that the energy separation of the ground state from the excited states is large, so that the field-induced mixing of the ground state with the excited states is negligible. To be able to compare the results of the calculations to existing experimental spectra, the polarization of the incident light $\hat{\boldsymbol{e}}_0$ is taken to be perpendicular to the electric field $\boldsymbol{F}$ and the incident photon energy distribution taken to be a 4 meV wide [full width at half maximum (FWHM)] Gaussian centered at the *zero-field* $1s^2 \rightarrow 1s6p\,{}^1P$ transition energy. This energy is held fixed when the field strength is increased.

By choosing the emitted photon energy region (i.e., the region covered by the spectrometer), we effectively narrow the number of different cascade paths we have to take into consideration in order to interpret the spectra. Here we study narrow energy intervals around the

$$1s6\ell \rightarrow 1s2p \qquad (2)$$

and

$$1s5\ell' \rightarrow 1s2p \qquad (3)$$

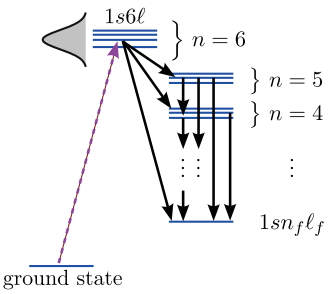

FIG. 1. (Color online) Radiative-decay cascades (solid black arrows) following photoexcitation (dashed arrow) to singly excited states of the $n = 6$ manifold in a static electric field.

transition energies. More specifically, at zero field, these energy regions are close to the $1s6d \rightarrow 1s2p$ and $1s5d \rightarrow 1s2p$ transition energies. We have taken into account that the $1s2p$ states (like the ground state) are only weakly perturbed by the field: energetically closest are the $1s2s$ states for which the energy separation from the $1s2p$ states is large in comparison with the coupling matrix elements due to the field for the field strengths considered here. Their influence on the $1s2p$ states can thus be neglected when interpreting the results. Furthermore, the $1s2p$ states are almost unaffected by the singlet-triplet coupling (see Sec. III A), so that transitions to these states reveal information about the singlet-triplet composition of the intermediate states. Thus, by comparison of experimental and theoretical emitted photon yields in the regions of the $1s6\ell \rightarrow 1s2p\,{}^1P$ ($1s5\ell' \rightarrow 1s2p\,{}^1P$) and $1s6\ell \rightarrow 1s2p\,{}^3P$ ($1s5\ell' \rightarrow 1s2p\,{}^3P$) transitions, the values of the calculated interaction matrix elements between various states due to the field and the calculated singlet-triplet coupling matrix elements can be checked.

For the two cases considered here [Eqs. (2) and (3)] the dominant contribution to the photon yields is expected to be due to the cascade paths with the lowest number of emission steps $\mathfrak{n}$, i.e., from the

$$1s^2 \xrightarrow[\text{(a)}]{\hbar\omega_0} 1s6\ell \xrightarrow[\text{(e)}]{\hbar\omega_1} 1s2p\,{}^{1,3}P \qquad (4)$$

and

$$1s^2 \xrightarrow[\text{(a)}]{\hbar\omega_0} 1s6\ell \xrightarrow[\text{(e)}]{\hbar\omega_1} 1s5\ell' \xrightarrow[\text{(e)}]{\hbar\omega_2} 1s2p\,{}^{1,3}P \qquad (5)$$

transitions. The first group of cascades [Eq. (4)] does not contribute to the total yield for $F = 0$ in the dipole approximation since the $1s6p \rightarrow 1s2p$ transitions are parity forbidden. On the contrary, cascades of the form given by Eq. (5) do contribute also in the case when no external field is applied.

III. THEORETICAL DESCRIPTION

A. States in an external electric field

The helium singly excited states $1sn\ell$ are usually described using LS- or LSJ-coupled basis states. The energy separation between manifolds with different principal quantum numbers of interest here ($n \lesssim 10$) is large compared to the magnitude of the singlet-triplet coupling matrix elements [9]. The largest relativistic corrections thus come from the singlet-triplet mixing between the states with the same n, L, and J, and this mixing is what we consider in the following.

It is customary to describe the coupling between the ${}^1L_L$ and ${}^3L_L$ states by the mixing angles θ_k ($0 \leqslant \theta_k \leqslant \pi/4$):

$$|\psi_k^+\rangle = \cos\theta_k |\psi_k^s\rangle + \sin\theta_k |\psi_k^t\rangle \qquad (6a)$$

$$= a_k^+ |\psi_k^s\rangle + b_k^+ |\psi_k^t\rangle, \qquad (6b)$$

$$|\psi_k^-\rangle = -\sin\theta_k |\psi_k^s\rangle + \cos\theta_k |\psi_k^t\rangle \qquad (7a)$$

$$= a_k^- |\psi_k^s\rangle + b_k^- |\psi_k^t\rangle, \qquad (7b)$$

where $|\psi_k^+\rangle$ denotes the energetically higher-lying state, which has a higher admixture of the singlet basis state $|\psi_k^s\rangle$, and $|\psi_k^-\rangle$ the lower-lying state, which has a higher admixture of the triplet basis state $|\psi_k^t\rangle$. If a singlet and a triplet state are only weakly mixed, θ_k is close to 0, and θ_k approaches $\pi/4$ if the mixing is strong. The mixing between the ^1L_L and ^3L_L states is almost complete for angular momenta $L \geqslant 3$ and is weak for $L = 1$ and $L = 2$ [9]. Note that the $^1S_0$, $^3S_1$, and $^3L_{L\pm1}$ basis states are not coupled to other states by the spin-orbit interaction, which means that these states have either purely singlet or purely triplet character. We will adopt the $^\pm L_J$ term notation for all the states for simplicity. It is to be understood that for the states not affected by the singlet-triplet mixing, "+" is used for the singlet and "−" for the triplet states.

The singlet-triplet coupling matrix element is

$$V_k = \langle \psi_k^s | V | \psi_k^t \rangle = \frac{E_k^s - E_k^t}{2} \tan 2\theta_k, \tag{8}$$

where E_k^s and E_k^t are the energies associated with the singlet basis state $|\psi_k^s\rangle$ and the triplet basis state $|\psi_k^t\rangle$. The eigenenergies pertaining to the states $|\psi_k^+\rangle$ and $|\psi_k^-\rangle$ are

$$E_k^\pm = \frac{E_k^s}{2}\left(1 \pm \frac{1}{\cos 2\theta_k}\right) + \frac{E_k^t}{2}\left(1 \mp \frac{1}{\cos 2\theta_k}\right). \tag{9}$$

It may be seen that the values of θ_k and $E_k^\pm$ depend critically on the exact values of V_k, E_k^s, and E_k^t. Since the singlet-triplet energy difference may be close to our numerical precision for high L and n, we take the values of $E_k^\pm$ and θ_k from the high-precision calculations (Refs. [9,10] and references therein) and write the Hamiltonian operator of the atom in the external field in the prediagonalized basis $\{|\psi_k^\pm\rangle\}$, thus avoiding possible numerical errors connected to the calculation of the exact energies of the spin-orbit mixed states. For $L \leqslant 7$, exact energies which incorporate corrections due to the finite nuclear mass are available (energies for ^{4}He; cf. Ref. [9]), and are used in the present calculations. The remaining energies are obtained by fitting a smooth, monotonic function to the L dependence of the quantum defects separately for each series of states (^+L_L, ^-L_L, $^-L_{L-1}$, and $^-L_{L+1}$) and extrapolating the values to $L = 8$ and $L = 9$. By this we make sure that level ordering is correct, which is crucial for the calculation of the atom-field interaction matrix elements.

The reduced dipole matrix elements are obtained from the equality

$$\begin{aligned}\langle \psi_k^w \| D \| \psi_{k'}^{w'} \rangle = a_k^w a_{k'}^{w'} \langle \psi_k^s \| D \| \psi_{k'}^s \rangle \\ + b_k^w b_{k'}^{w'} \langle \psi_k^t \| D \| \psi_{k'}^t \rangle,\end{aligned} \tag{10}$$

where w and w' stand for $+$ or $-$. The dipole matrix elements between the LSJ-coupled states $\langle \psi_k^{s,t} \| D \| \psi_{k'}^{s,t} \rangle$ have been taken from configuration-interaction (CI) calculations similar to the calculations from Ref. [11]: where comparison is possible, the relative differences between the CI and high-precision calculation oscillator strengths [9] for transitions between pairs of states are not higher than 1.2×10^{-4}. These differences decrease with increasing n and L, and are largest for the energetically lowest states.

The Hamiltonian operator of the atom in the external electric field $\boldsymbol{F}$ aligned along the z axis is

$$H = H_0 + V_F = H_0 + F(z_1 + z_2), \tag{11}$$

where H_0 is the Hamiltonian operator of the free atom (including the relativistic terms), V_F is the atom-field interaction, and z_1 and z_2 are the electron coordinates along the direction of the field. For our present choice of the coordinate system, the field couples only atomic states with equal projections of the angular momenta ($M_k = M_{k'} = M$):

$$\langle \psi_k^w | V_F | \psi_{k'}^{w'} \rangle = F\,(-1)^{J_k - M} \begin{pmatrix} J_k & 1 & J_{k'} \\ -M & 0 & M \end{pmatrix} \langle \psi_k^w \| D \| \psi_{k'}^{w'} \rangle. \tag{12}$$

Our basis set consists of states $|\psi_k^\pm\rangle$ with $n \leqslant 10$ and $L \leqslant 9$. For each value of the field strength F and projection M, we solve the eigenvalue problem

$$H|\Psi_a\rangle = E_a|\Psi_a\rangle, \tag{13}$$

$$|\Psi_a\rangle = \sum_{w,k} c_a^{w,k} |\psi_k^w\rangle \,(M_k = M), \tag{14}$$

where $|\Psi_a\rangle$ and E_a denote the eigenstate in the external field and the corresponding eigenvalue.

Although the prediagonalized basis is used in the calculation, it is still useful to think in terms of the LSJ-coupled basis states $\{|\psi_k^{s,t}\rangle\}$ when interpreting the spectra. In our case, the excitation proceeds from the ground state, which is well separated from the excited states. This means that the field-induced mixing with these states can be neglected for the field strengths considered here ($F \lesssim 10$ kV/cm), and we may assume that the initial state has $^1S_0$ symmetry. In the dipole approximation, an accessible excited state must thus have a nonzero admixture of the $^1P_1$ component (Fig. 2). The higher-angular-momentum ^1L_L states then participate through the coupling with the $^1P_1$ basis states. The dominant mechanism for accessing the triplet states is the almost complete ($\theta_k \approx \pi/4$) singlet-triplet mixing of the ^1L_L states with the ^3L_L states for $L \geqslant 3$. Note here that the mixing coefficients for the P_1 and D_2 states are small: $\sin\theta_k \lesssim 2.8 \times 10^{-4}$ for the P_1 and $\sin\theta_k \lesssim 1.6 \times 10^{-2}$ for the D_2 states [9], which means that

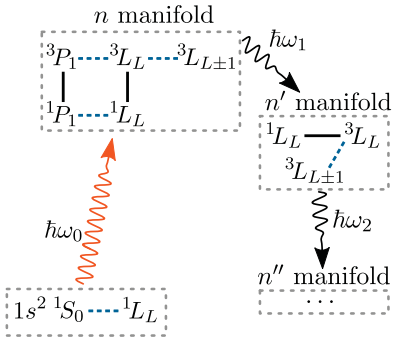

FIG. 2. (Color online) Photoexcitation of the ground-state He atom in an external electric field (see text). The solid lines denote the singlet-triplet coupling and the dashed lines the field-induced coupling. Photoabsorption ($\hbar\omega_0$) and photon emission (the first and the second steps, $\hbar\omega_1$ and $\hbar\omega_2$) are depicted with wavy lines.

the ${}^{\pm}P_1$ and ${}^{\pm}D_2$ states have almost exclusively singlet or exclusively triplet character. Notable singlet-triplet mixing can thus be achieved only through the states with higher angular momenta. Furthermore, in the next order, the field couples the ${}^3L_L$ and the ${}^3L_{L\pm1}$ states. It should be stressed that, even though the latter states are not strongly mixed with the rest of the LSJ-coupled basis states after photoexcitation, they can nevertheless be populated during radiative cascades.

B. Description of radiative-decay cascades

The singly excited states considered here are characterized by energy widths which are narrow in comparison with the energy differences between the states of the same manifold. Interference effects which originate from the energy overlap of these states can therefore be neglected. In this case, absorption and $\mathfrak{n}$ subsequent emission steps are treated as independent processes. The probability of emitting several photons is then written as a product of probabilities for photon emission in each individual step. The number of photons emitted in the energy region between ω and $\omega + d\omega$ is proportional to the differential cross section:

$$\frac{d\sigma}{d\omega} = \sum_f \sum_{\mathfrak{n}} \sum_{a_1,\ldots,a_{\mathfrak{n}}} \sigma^{\mathrm{int}}_{a_1,g}\, T(\omega_c - E_g + E_{a_1}) \times \left(\prod_{j=1}^{\mathfrak{n}-1} \frac{\Gamma_{a_{j+1},a_j}}{\Gamma_{a_j}} \right) \frac{\Gamma_{f a_{\mathfrak{n}}}}{\Gamma_{a_{\mathfrak{n}}}} \times \frac{\Gamma_{a_{\mathfrak{n}}}/(2\pi)}{(E_f + \omega - E_{a_{\mathfrak{n}}})^2 + \Gamma^2_{a_{\mathfrak{n}}}/4}, \tag{15}$$

where T is the incident photon energy distribution centered at energy ω_c, $\mathfrak{n}$ is the number of emission steps following photoabsorption in a cascade leading to a final state $|\Psi_f\rangle$ through intermediate states $|\Psi_{a_1}\rangle, \ldots, |\Psi_{a_{\mathfrak{n}}}\rangle$, and

$$\sigma^{\mathrm{int}}_{a_1,g} = 4\pi^2 \alpha\, (E_{a_1} - E_g)\, |\langle \Psi_{a_1} | \hat{\boldsymbol{e}}_0 \cdot (\boldsymbol{r}_1 + \boldsymbol{r}_2) | \Psi_g \rangle|^2 \tag{16}$$

is the energy-integrated cross section for linearly polarized incident light (polarization $\hat{\boldsymbol{e}}_0$) which describes photoexcitation from the ground state $|\Psi_g\rangle$ to the state $|\Psi_{a_1}\rangle$. Electron coordinates are denoted by $\boldsymbol{r}_1$ and $\boldsymbol{r}_2$, and the energies of the ground state, intermediate states, and final states by E_g, E_{a_1}, ..., $E_{a_{\mathfrak{n}}}$, and E_f, respectively. We have used Γ_{ab} for the partial widths describing spontaneous decays from $|\Psi_b\rangle$ to $|\Psi_a\rangle$, and Γ_b for the total widths of the intermediate states:

$$\Gamma_{ab} = \frac{4\alpha^3}{3} (E_b - E_a)^3 |\langle \Psi_a | \mathcal{D}_{M_a - M_b} | \Psi_b \rangle|^2, \tag{17}$$

$$\Gamma_b = \sum_a \Gamma_{ab}, \tag{18}$$

$$\mathcal{D}_q = \sqrt{4\pi/3}\, \{ r_1 Y_{1q}(\hat{\boldsymbol{r}}_1) + r_2 Y_{1q}(\hat{\boldsymbol{r}}_2) \}. \tag{19}$$

We have taken into account that the distribution T is broad in comparison with the energy widths, so that $T(\omega_0)$ has been regarded as constant around the resonance energies $\omega_0 = E_{a_1} - E_g$.

Equation (15) can be interpreted as follows. Excitation into various states $|\Psi_{a_1}\rangle$ is described by the weighted photoexcitation cross section $\sigma^{\mathrm{int}}_{a_1,g} T(\omega_c - E_g + E_{a_1})$, and the product in the parentheses and the subsequent factor describe the branching ratios for the cascade $|\Psi_{a_1}\rangle \to \cdots \to |\Psi_{a_{\mathfrak{n}}}\rangle \to |\Psi_f\rangle$. The Lorentzian factor at the end of Eq. (15) describes the spread of the energy of the last ($\mathfrak{n}$th) emitted photon we measure. Note that Eq. (15) includes contributions of cascades with various number of steps $\mathfrak{n}$, so that the system may arrive at the final state after emitting one ($\mathfrak{n} = 1$), two ($\mathfrak{n} = 2$), three ($\mathfrak{n} = 3$), etc. photons.

For $\boldsymbol{F} \parallel \hat{\boldsymbol{z}}$, a state $|\Psi_a(M)\rangle$ with the projection $M > 0$ is degenerate with the analogous state $|\Psi_a(-M)\rangle$. These two states have equal energy widths and obviously overlap in energy. It should be stressed, however, that Eq. (15) is still valid since the cascades which involve the $|\Psi_a(+M)\rangle$ state end in *different final dressed atomic states* than cascades which involve the $|\Psi_a(-M)\rangle$ state. In other words, it is possible—at least in principle—to determine through which of these states the cascade decay proceeds by measuring polarization of the emitted photons.

IV. RESULTS AND DISCUSSION

A. Inelastic photon scattering cross section

In Sec. III B, we treated absorption and each of the emission steps as independent processes. Contributions stemming from various cascades with equal numbers of steps $\mathfrak{n}$ starting in the same initial state and ending in the same final state in Eq. (15) are written in the form of an *incoherent* sum. It is instructive to compare these cross sections with the inelastic photon scattering cross sections calculated with the Kramers-Heisenberg formula [12]:

$$\frac{d\sigma^{(1)}}{d\omega} = \alpha^4 \omega^3 \sum_f (E_f + \omega - E_g) \sum_\beta \int d\Omega |\mathcal{M}^{(\beta)}_{fg}|^2 \times T(\omega_c - E_f - \omega + E_g), \tag{20}$$

$$\mathcal{M}^{(\beta)}_{fg} = \sum_a \frac{\langle \Psi_f | D(\hat{\boldsymbol{e}}_\beta) | \Psi_a \rangle \langle \Psi_a | D(\hat{\boldsymbol{e}}_0) | \Psi_g \rangle}{E_f + \omega - E_a + i\Gamma_a/2}, \tag{21}$$

where $D(\hat{\boldsymbol{e}}) = \hat{\boldsymbol{e}} \cdot (\boldsymbol{r}_1 + \boldsymbol{r}_2)$ is the dipole operator. In Eq. (20), we have summed over the two independent polarization directions ($\hat{\boldsymbol{e}}_\beta$) and integrated over the directions of the emitted photons. The factor $T(\omega_c - E_f - \omega + E_g)$ results from the convolution with the incident photon energy distribution.

The cross sections from Eq. (20) correspond to the case of $\mathfrak{n} = 1$ in Eq. (15), with the exception that in Eqs. (20) and (21) the contributions of various intermediate states $|\Psi_a\rangle$ are summed in a *coherent* way. This may result in differences between the cross sections calculated with Eq. (15) and the cross sections calculated with Eq. (20) in the energy regions between the resonances, where interference effects may become important. These differences are summarized in Fig. 3. The main discrepancies between Eqs. (15) and (20) are due to cancellation of contributions from neighboring intermediate states. This effect is most pronounced in the regions between the resonance energies, where the contributing terms from Eq. (21) are of the same order of magnitude. Furthermore, two additional peaks appear in the incoherent case [Eq. (15)] at 414.54 and 414.65 nm, which is due to the cascades with more than one emission step ($\mathfrak{n} \geqslant 2$) not included in Eq. (20). The extremely small differences

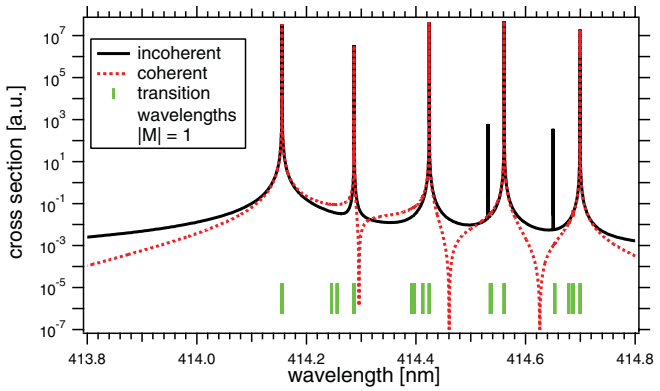

FIG. 3. (Color online) Theoretical cross sections calculated using Eq. (15) (incoherent, solid black) for $\mathfrak{n} \leqslant 10$ and Eqs. (20) and (21) (coherent, dotted red) in the region of the $1s6\ell \rightarrow 1s2p\,{}^+P_1$ transitions for $\hat{\boldsymbol{e}}_0 \perp \boldsymbol{F}$ and electric field strength of 9.17 kV/cm. The central energy of the incident photon energy distribution (Gaussian, 4 meV FWHM) is tuned to match the zero-field energy of the $1s^2 \rightarrow 1s6p\,{}^+P_1$ transitions. Green (gray) bars mark transition wavelengths from the accessible $1s6\ell$ states to the $1s2p\,{}^+P_1$ states.

between the incoherent and coherent results and simpler application of the former especially for the cascades comprising many emission steps fully justify the incoherent modeling approach.

B. Testing the theoretical model for the singlet ($^+P_1$) final states

To some extent we can check the validity of the theoretical model by comparing the calculated spectra to the high-resolution data taken for calibration purposes in the previous experiments on doubly excited states [13–15]. These spectra were acquired at the Gas Phase Photoemission beamline at Elettra synchrotron light source, Italy, in the region of the $1s6\ell \rightarrow 1s2p\,{}^+P_1$ and the $1s5\ell' \rightarrow 1s2p\,{}^+P_1$ transitions.

The measured (points) and the calculated (solid lines) photon-yield spectra from the wavelength region of the $1s6\ell \rightarrow 1s2p\,{}^+P_1$ transitions are shown in Fig. 4. These photon yield spectra correspond to Eq. (2) for the case of the $^+P_1$ (singlet) final states. Excellent agreement is obtained if the theoretical spectra are broadened by a Gaussian distribution of 0.38 meV FWHM, which accounts for the spectrometer response. We found that the experimental field strengths had to be multiplied by a correction factor of 0.92 to match the theoretical energy splitting of the peaks within the $1s6\ell$ multiplet. This correction factor takes into account mechanical tolerances and field penetration effects (similar to those described in Ref. [7]). Although Fig. 4 shows the total yield from cascades with $\mathfrak{n} \leqslant 10$, the calculations confirm that the dominant contribution is due to the single-step processes ($1s^2 \rightarrow 1s6\ell \rightarrow 1s2p\,{}^+P_1$). As has already been pointed out, this wavelength region contains no spectral lines which correspond to dipole transitions for $F = 0$ and $\mathfrak{n} = 1$. Indeed, the 0 kV/cm spectrum (not shown) contains no measurable signal. The preservation of the $^+S_0$ ground-state symmetry (discussed in Sec. III A) assures that only the $1s6p\,{}^+P_1$ components of the states in the external field are reached through the dipole excitation. However, since the $1s2p$

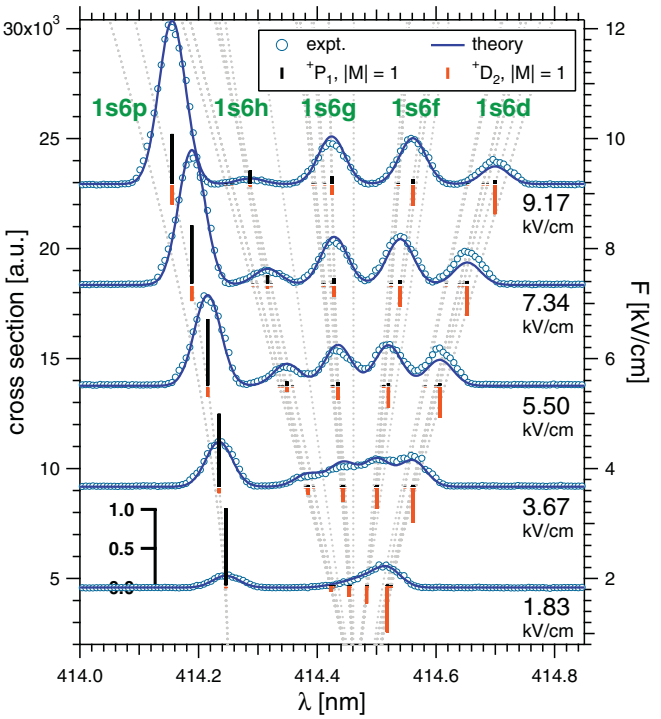

FIG. 4. (Color online) Experimental (points) and theoretical (solid line) cross sections $d\sigma/d\omega$ for $\boldsymbol{F} \perp \hat{\boldsymbol{e}}_0$ in the region of the $1s6\ell \rightarrow 1s2p\,{}^+P_1$ transitions (see text for notation). The central energy of the incident photon energy distribution (Gaussian, 4 meV FWHM) is tuned to match the zero-field energy of the $1s^2 \rightarrow 1s6p\,{}^+P_1$ transitions. The baselines of the spectra are offset to match the field value (the right axis). A single scaling factor is used to match the experimental and theoretical scales. The theoretical spectra are broadened with a Gaussian distribution with 0.38 meV FWHM to account for the finite resolution of the spectrometer. The black and orange (gray) bars show the weights (inset scale) of the $^+P_1$ and $^+D_2$ components of the states accessible with photoexcitation. The light-gray dotted lines show the evolution of the $1s6\ell$ state energies with the field strength.

states are only weakly mixed with other states due to the large energy separation and the $1s6p \rightarrow 1s2p$ transition is dipole forbidden, the measured emission signal could originate from the admixture of either the $1s6s$ or the $1s6d$ singlet basis states. Since $\hat{\boldsymbol{e}}_0 \perp \boldsymbol{F}$, the projections M_{a_1} of the excited states are restricted to ± 1. The admixture of the $1s6s$ basis state is therefore zero, and the measured emission signal originates from the $1s6d\,{}^+D_2$ states alone. The strength of the emission lines is therefore interpreted by considering: (i) the admixture of the $1s6p\,{}^+P_1$ basis states in the excitation step, and (ii) the admixture of the $1s6d\,{}^+D_2$ basis states in the emission step. This is depicted in Fig. 4 with black and orange (gray) bars which show the weights of the $^+P_1$ and $^+D_2$ basis states, respectively. The peaks, which may be clearly resolved for field strengths $F \gtrsim 2$ kV/cm, are due to the admixture of the $^+P_1$ and $^+D_2$ components in the $F \neq 0$ states. Only where both of these components are different from zero is there a nonzero contribution to the photon yield. The calculations show that the singlet-triplet coupling is not essential to reproduce these experimental yields: virtually identical spectra

are obtained if the singlet-triplet coupling is neglected. Since the singlet-triplet splitting is small in comparison with the experimental resolution (the widths of both the excitation and the spectrometer energy distributions), only the total singlet dipole strength—additionally redistributed across the $n = 6$ multiplet because of the singlet-triplet coupling—is relevant.

An additional remark concerns the angular dependence of the emitted photon yields. For the experimental setup of Ref. [13], with $\boldsymbol{F} \perp \hat{\boldsymbol{e}}_0$, those photons are detected which are emitted into mirrored cones lying in a plane perpendicular to $\boldsymbol{F}$, with their axes parallel to $\hat{\boldsymbol{e}}_0$. For the $1s^2 \rightarrow 1s6\ell \rightarrow 1s2p\,{}^+P_1$ spectra, the calculations indicate that the ratios of the spectral line amplitudes do not depend on the magnitude of the solid angle covered by the detector: changing the solid angle affects only the overall magnitudes of the peaks. This can be understood in the following way. For each of the $1s6\ell$ peaks, the only contribution stems from the admixture of the $1s6d\,{}^+D_2$ basis states, which means that the angular dependence of the emission signal is the same for all the states for a particular field strength.

The second test case, which corresponds to Eq. (3), is shown in Fig. 5, where the calculated cross sections are compared to the experimental data in the wavelength region of the $1s5\ell' \rightarrow 1s2p\,{}^+P_1$ transitions. Overall agreement between the calculated and measured spectra is good, with the discrepancies attributed to the uncertainties in the experimental conditions, particularly to polarization-dependent spectrometer efficiency

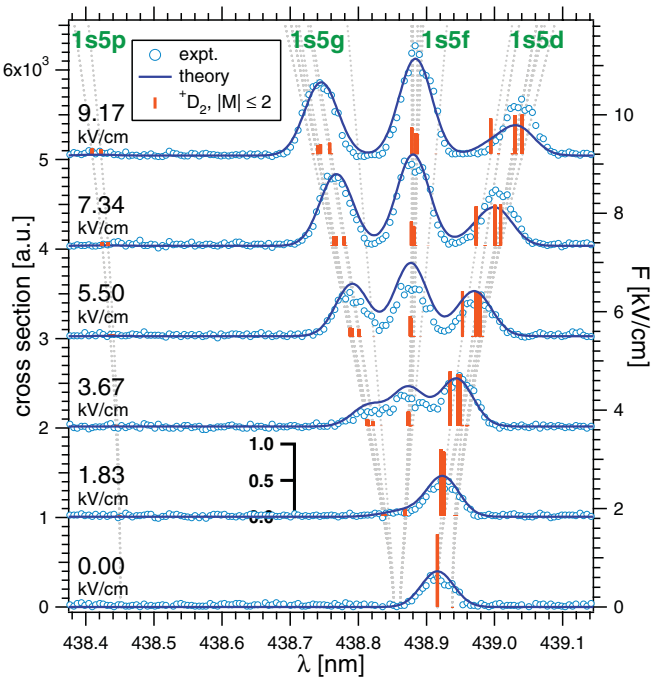

FIG. 5. (Color online) Experimental (points) and theoretical (solid line) cross sections $d\sigma/d\omega$ for $\boldsymbol{F} \perp \hat{\boldsymbol{e}}_0$ in the region of the $1s5\ell \rightarrow 1s2p\,{}^+P_1$ transitions. The central energy of the incident photon energy distribution (Gaussian, 4 meV FWHM) is tuned to the zero-field $1s^2 \rightarrow 1s6p\,{}^+P_1$ transition energy. The bars show the weights of the $^+D_2$ components of the $n = 5$ states accessible after the first emission step. The spectrometer broadening is described by a Gaussian distribution (0.36 meV FWHM).

and to uncertainties in the magnitude of the detector solid angle. As expected, the dominant signal originates from the transitions $1s^2 \rightarrow 1s6\ell \rightarrow 1s5\ell' \rightarrow 1s2p\,{}^+P_1$. Note that, in contrast to the previous case, a peak is observed here for $F = 0$ as well since dipole transitions from the $1s5s$ and $1s5d$ states to the $1s2p$ states are allowed. However, photons emitted from the field-modified $1s5s$ states lie outside the observed interval ($\lambda \approx 443.8$ nm). Only the weights of the $1s5d$ singlet basis states are thus shown in Fig. 5, since the admixture of the $1s5s$ basis state is small, due to the large energy separation from the rest of the multiplet.

C. Theoretical predictions

The emitted photon yields for the cascades which end in the $1s2p\,{}^+P_1$ final states are enhanced when a nonzero electric field is applied. For the two cases considered in Sec. IV B, the inclusion of the singlet-triplet mixing is not essential to reproduce the spectral features. The latter does not hold for the cascades which end in the $1s2p\,{}^-P_{J_f}$ ($0 \leqslant J_f \leqslant 2$) final states, i.e., in the triplet final states. These cascades are "doubly forbidden" in the sense that, in the zero field or without the singlet-triplet mixing, no signal can be recorded in the first emission step ($\mathfrak{n} = 1$) of the cascade. This means that a combined effect of the singlet-triplet mixing and the field-induced mixing of the $1s6\ell$ states may be directly observed if the $1s^2 \rightarrow 1s6\ell \rightarrow 1s2p\,{}^-P_{J_f}$ transitions are studied, since the first emission step dominates the signal. Future experimental detection of the fluorescence in this wavelength region under similar excitation conditions would therefore represent a fingerprint of the combined effect of the external field and the singlet-triplet coupling. Figure 6 shows the calculated spectra in the region of the $1s6\ell \rightarrow 1s2p\,{}^-P_{J_f}$ transitions. The amplitude of the largest peak in Fig. 6 ($1s6h$) is calculated to be approximately 70 times lower than the amplitude of the $1s6p$ peak in Fig. 4 for the field strength of 9.17 kV/cm. As before, excitation to a chosen state is possible through the admixture of the $^+P_1$ basis states, but here the admixture of the ^-D_J states determines the emission strength. The weights of the $^+P_1$ and ^-D_J states are plotted in Fig. 6 with black and orange (gray) bars, respectively. Although dipole transitions to the final states are also possible in this case through the mixing with the $^-S_1$ basis states, the weights of these states are several orders of magnitude lower than the ^-D_J weights. The reason for this is that the $1s6s$ states are energetically separated from the rest of the $n = 6$ multiplet.

We also examine the region pertaining to the $1s5\ell' \rightarrow 1s2p\,{}^-P_{J_f}$ transitions. As for the singlet final states, the signal stems predominantly from the $\mathfrak{n} = 2$ transitions $1s^2 \rightarrow 1s6\ell \rightarrow 1s5\ell' \rightarrow 1s2p\,{}^-P_{J_f}$. The results of the calculations are shown in Fig. 7. Although the $F = 0$ spectrum contains contributions pertaining to the $1s5d\,{}^-D_J \rightarrow 1s2p\,{}^-P_{J_f}$ transitions, this signal is relatively weak: the amplitude due to these transitions in the convoluted spectrum is approximately 540 times lower than the amplitude of the largest ($1s5g$) peak at 9.17 kV/cm. The amplitude of the $1s5g$ peak is about 20 times lower than the signal of the singlet transitions at the same field strength and 150 times lower than the amplitude of the $1s6p$ peak at 9.17 kV/cm from Fig. 7.

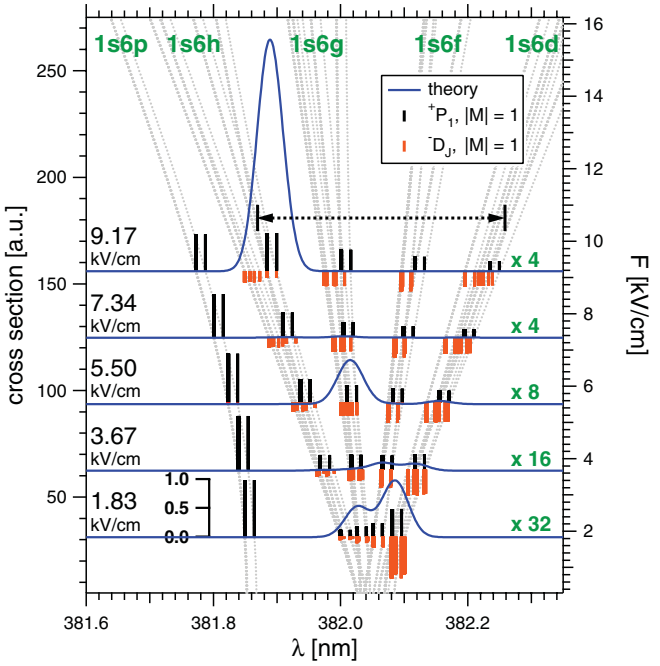

FIG. 6. (Color online) Theoretical cross sections in the region of the $1s6\ell \rightarrow 1s2p\,^{-}P_{J_f}$ transitions for $\boldsymbol{F} \perp \hat{\boldsymbol{e}}_0$ and the central energy of the incident photons ω_c tuned to the zero-field $1s^2 \rightarrow 1s6p\,^{+}P_1$ transitions. The black and orange (gray) bars show the $^{+}P_1$ and $^{-}D_J$ weights of the accessible $n = 6$ states. The spectra have been broadened by a Gaussian profile with 0.38 meV FWHM. Except for the $1s6p$ parts, the magnitudes of the $^{+}P_1$ bars have been multiplied for visibility by the factors given in the figure (right). Note that the cross sections are not scaled.

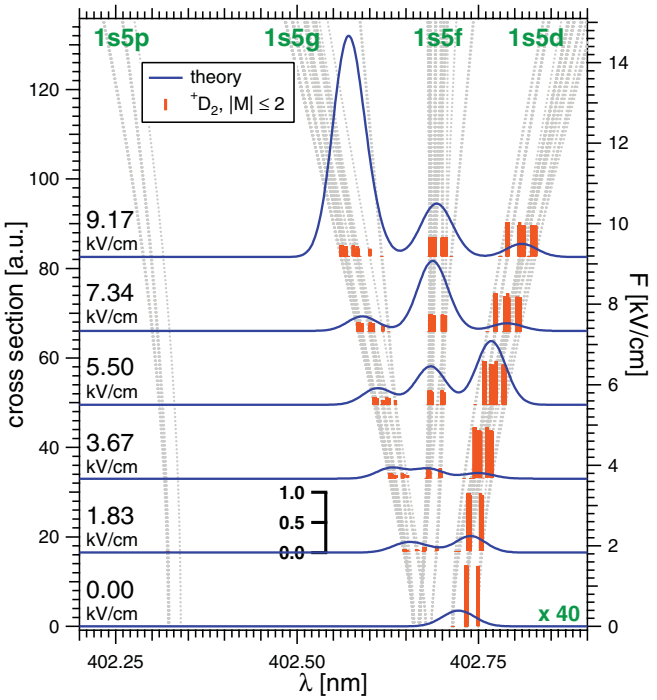

FIG. 7. (Color online) Experimental (points) and theoretical (solid line) cross sections $d\sigma/d\omega$ for $\boldsymbol{F} \perp \hat{\boldsymbol{e}}_0$ in the region of the $1s5\ell \rightarrow 1s2p\,^{-}P_J$ transitions. The central energy of the incident photon energy distribution (Gaussian, 4 meV FWHM) is tuned to the zero-field $1s^2 \rightarrow 1s6p\,^{+}P_1$ transition energy. The bars show the weights of the $^{-}D_J$ components of the $n = 5$ states accessible after the first emission step. The spectrometer broadening is described by a Gaussian distribution (0.36 meV FWHM).

As can be seen from Figs. 6 and 7, the peak amplitudes may change nonmonotonically with the field strength, which is a consequence of an intricate dependence of the energies and the compositions of the field-modified states (in terms of the field-free states) on the field strength. Because of the relatively large number of states involved, this dependence becomes complex and is especially nontrivial close to avoided crossings.

For both cases considered here, the exact peak amplitudes and their positions are very sensitive to small variations in the state energies and the magnitudes of the dipole matrix elements. In particular, neglecting the energy differences between the $^{-}L_{L-1}$ and $^{-}L_{L+1}$ states (i.e., setting these energies to be equal) results in photon-yield spectra where the amplitude of the $1s6p$ peak for the $1s2p\,^{+}P_1$ final states is about 120 times the amplitude of the $1s6h$ peak for the $1s2p\,^{-}P_J$ final states at 9.17 kV/cm. At the same field strength, the amplitude of the $1s5g$ peak in the singlet spectrum is approximately 30 times the amplitude of the $1s5g$ peak for the case of the $1s2p\,^{-}P_J$ final states. This latter peak is about a factor of 340 larger than the $F = 0$ $1s5d$ peak. All this indicates that photon-yield measurements in an external electric field could provide a very stringent test for the calculated energies and the dipole transition amplitudes. The measured photon yields which result from transitions to predominantly triplet states can thus provide experimental information on the strengths of both the singlet-triplet mixing and the field-induced coupling of the states with higher angular momenta.

V. CONCLUSIONS

We have presented a theoretical framework for the simulation of radiative cascades from the singly excited states of the helium atom in a static electric field, taking full account of the singlet-triplet mixing. Simulations of the energy-resolved fluorescence yield associated with the triplet final $1s2p$ states show a strong signal enhancement in the triplet channel that occurs for nonzero field. The transfer of intensity from the singlet channel is mediated by the high-angular-momentum states which are characterized by strong singlet-triplet mixing and couple to the low-angular-momentum states in the presence of the field. The LS-coupling scheme is seen to be a good approximation for the description of the helium singly excited states with low angular momenta, and the population of the triplet states by photon impact excitation of atoms in the singlet ground state is not very likely to occur. Application of moderate electric fields may help detect transitions to the triplet states and may enable studies of the singlet-triplet mixing strengths by observation of the fluorescence cascade decay.

The present theoretical approach is obviously adequate for the description of singlet-triplet mixing between the singly excited states also in zero electric field. To reach firm

conclusions about the relative importance of singlet-triplet mixing in singly and doubly excited states, which affects the experimental results of Ref. [8], accurate modeling of the singlet-triplet mixing between doubly excited states is needed.

APPENDIX: EXCITATION STRENGTHS AND PARTIAL WIDTHS OF THE $1s6\ell$ STATES

In Table I we report energy-integrated excitation cross sections [Eq. (16)], total widths, and partial widths of the $1s6\ell \rightarrow 1s2p$ transitions in an external field. The total energy widths are calculated by using Eqs. (17)–(19) and the partial widths by means of

$$\Gamma_a^{\pm} = \frac{4\alpha^3}{3} \sum_{f_\pm} (E_a - E_{f_\pm})^3 |\langle \Psi_{f_\pm} | \mathcal{D}_{M_{f_\pm} - M_a} | \Psi_a \rangle|^2, \qquad \text{(A1)}$$

where Γ_a^+ (Γ_a^-) denotes the decay width of a field-modified $1s6\ell$ state $|\Psi_a\rangle$ to the field-modified $1s2p\ ^+P_1$ states $|\Psi_{f_+}\rangle$ ($1s2p\ ^-P_{0,1,2}$ states $|\Psi_{f_-}\rangle$). The energies of the states $|\Psi_a\rangle$ and $|\Psi_{f_\pm}\rangle$ are denoted by E_a and $E_{f_\pm}$, respectively. For completeness, the widths of the $1s6\ell \rightarrow 1s2p$ transitions for $F = 0$ are also reported in Table II.

TABLE I. The energies E_a, total widths Γ_a, and partial widths $\Gamma_a^\pm$ of the field-modified $1s6\ell$ states with $|M_a| \leqslant 1$ for the field strength $F = 9.17$ kV/cm. The numbers in square brackets denote the powers of ten. All quantities are given in atomic units. The energy-integrated cross sections $\sigma_{ag}^{\rm int}$ are calculated for the case of $\hat{\boldsymbol{e}}_0 \parallel \boldsymbol{F}$ ($M_a = 0$) and for the case of $\hat{\boldsymbol{e}}_0 \perp \boldsymbol{F}$ ($M_a = \pm 1$).

$\lvert M_a\rvert$	$-E_a$	$\sigma_{ag}^{\rm int}$	Γ_a	Γ_a^+	Γ_a^-
1	2.0153797774	1.76[−15]	1.36[−10]	1.19[−18]	5.90[−11]
0	2.0153797774	0	1.36[−10]	1.19[−18]	5.90[−11]
0	2.0145670181	6.96[−06]	1.14[−10]	4.40[−11]	4.36[−18]
1	2.0142136879	1.68[−11]	7.42[−11]	1.84[−19]	2.61[−12]
0	2.0142136819	7.24[−11]	7.42[−11]	8.22[−19]	2.61[−12]
0	2.0142136357	0	7.44[−11]	1.76[−21]	2.89[−12]
1	2.0142135640	2.03[−11]	7.52[−11]	4.30[−19]	3.61[−12]
0	2.0142134742	0	7.49[−11]	9.58[−20]	3.34[−12]
0	2.0139570463	6.62[−05]	2.24[−10]	4.65[−11]	1.11[−16]
1	2.0139530703	2.68[−05]	2.03[−10]	4.37[−11]	4.84[−16]
1	2.0139496656	3.45[−10]	1.21[−10]	4.21[−16]	3.89[−11]
0	2.0139496622	0	1.21[−10]	3.84[−19]	3.89[−11]
0	2.0139477051	2.79[−10]	1.21[−10]	9.88[−17]	3.98[−11]
1	2.0139477020	3.51[−11]	1.21[−10]	2.84[−17]	3.98[−11]
0	2.0139476983	0	1.21[−10]	6.07[−19]	3.98[−11]
1	2.0139408813	2.19[−11]	1.22[−10]	2.15[−17]	4.17[−11]
0	2.0139179922	8.22[−05]	2.04[−10]	2.75[−11]	7.22[−17]
1	2.0139163600	3.86[−05]	1.99[−10]	3.00[−11]	1.42[−16]
1	2.0139100419	1.10[−10]	1.00[−10]	3.82[−17]	4.25[−11]
0	2.0139100393	0	1.00[−10]	3.65[−19]	4.25[−11]
0	2.0139099382	3.15[−10]	1.03[−10]	4.05[−17]	4.47[−11]
1	2.0139099357	2.96[−11]	1.03[−10]	6.58[−18]	4.47[−11]
0	2.0139099322	0	1.03[−10]	7.37[−19]	4.47[−11]
1	2.0139096167	7.92[−11]	1.15[−10]	4.11[−17]	5.47[−11]
0	2.0138802957	1.13[−04]	2.36[−10]	1.23[−11]	6.07[−17]
1	2.0138800742	5.73[−05]	2.40[−10]	1.39[−11]	2.48[−16]
1	2.0138770124	4.28[−10]	1.03[−10]	7.68[−17]	4.07[−11]
0	2.0138728346	4.51[−10]	1.00[−10]	1.08[−17]	4.06[−11]
1	2.0138728322	2.83[−11]	1.00[−10]	6.44[−19]	4.06[−11]
0	2.0138728293	0	1.00[−10]	6.11[−19]	4.06[−11]
1	2.0138716591	1.10[−10]	9.90[−11]	4.21[−18]	4.02[−11]
0	2.0138716563	0	9.90[−11]	4.07[−19]	4.02[−11]
1	2.0138437214	1.03[−04]	3.67[−10]	1.08[−12]	1.01[−13]
1	2.0138436280	5.71[−07]	9.69[−11]	5.79[−15]	1.84[−11]
0	2.0138423108	1.84[−04]	3.37[−10]	1.15[−12]	5.82[−17]
0	2.0138354094	9.42[−10]	1.08[−10]	1.45[−18]	2.79[−11]
1	2.0138354067	5.00[−11]	1.08[−10]	1.58[−18]	2.79[−11]
0	2.0138354039	0	1.08[−10]	4.22[−19]	2.79[−11]
1	2.0138327525	2.27[−10]	1.11[−10]	4.20[−18]	3.06[−11]
0	2.0138327496	0	1.11[−10]	3.09[−19]	3.06[−11]
1	2.0138087468	3.95[−04]	1.24[−09]	2.93[−11]	4.19[−17]
0	2.0138006114	7.89[−04]	1.24[−09]	3.09[−11]	3.32[−17]

TABLE II. The energies E_a, total widths Γ_a, and partial widths $\Gamma_a^{\pm}$ of the $1s6\ell \rightarrow 1s2p$ transitions for $F = 0$. The energy-integrated cross sections $\sigma_{ag}^{\rm int}$ of the $1s6p\ ^+P_1$ states are 1.242×10^{-3} a.u. for $\hat{\boldsymbol{e}}_0 \parallel \boldsymbol{F}$ ($M_a = 0$) and 6.212×10^{-4} a.u. for $\hat{\boldsymbol{e}}_0 \perp \boldsymbol{F}$ ($M_a = \pm 1$), and the cross sections of the $1s6p\ ^-P_1$ states are 7.515×10^{-11} a.u. ($\hat{\boldsymbol{e}}_0 \parallel \boldsymbol{F}$) and 3.758×10^{-11} a.u. ($\hat{\boldsymbol{e}}_0 \perp \boldsymbol{F}$).

$\lvert M_a \rvert$	${}^wL_J$	$-E_a$	Γ_a	Γ_a^+	Γ_a^-
0,1	${}^-S_1$	2.0153776857	1.36[−10]	1.19[−18]	5.92[−11]
0	${}^+S_0$	2.0145631337	1.04[−10]	4.42[−11]	4.38[−18]
0,1	${}^-D_3$	2.0139014510	2.34[−10]	0	1.56[−10]
0,1	${}^-D_2$	2.0139014493	2.34[−10]	1.13[−14]	1.56[−10]
0,1	${}^-D_1$	2.0139014244	2.34[−10]	3.93[−18]	1.56[−10]
0,1	${}^+D_2$	2.0138982650	1.96[−10]	1.18[−10]	1.48[−14]

[1] M. Alagia, M. Coreno, H. Farrokhpour, P. Franceschi, A. Mihelič, A. Moise, R. Omidyan, K. C. Prince, R. Richter, J. Söderström, S. Stranges, M. Tabrizchi, and M. Žitnik, Phys. Rev. Lett. **102**, 153001 (2009).

[2] A. Moise, M. Alagia, L. Banchi, M. Ferianis, K. C. Prince, and R. Richter, Nucl. Instrum. Methods Phys. Res., Sect. A **588**, 502 (2008).

[3] M. Nagasono, E. Suljoti, A. Pietzsch, F. Hennies, M. Wellhöfer, J.-T. Hoeft, M. Martins, W. Wurth, R. Treusch, J. Feldhaus, J. R. Schneider, and A. Föhlisch, Phys. Rev. A **75**, 051406 (2007).

[4] J. S. Foster, Phys. Rev. **23**, 667 (1924).

[5] J. S. Foster, Proc. R. Soc. London, Ser. A **117**, 137 (1927).

[6] E. Schrödinger, Ann. Phys. (Berlin) **385**, 437 (1926).

[7] J. R. Harries and Y. Azuma, Rev. Sci. Instrum. **75**, 4406 (2004).

[8] J.-E. Rubensson, A. Moise, A. Mihelič, K. Bučar, M. Žitnik, and R. Richter, Phys. Rev. A **81**, 062510 (2010).

[9] G. W. F. Drake, in *Handbook of Atomic, Molecular, and Optical Physics*, edited by G. W. F. Drake (Springer, Berlin, 2006) Chap. B.11, pp. 199–219.

[10] R. El-Wazni and G. W. F. Drake, Phys. Rev. A **80**, 064501 (2009).

[11] A. Mihelič, Ph.D. Thesis, University of Ljubljana, 2006.

[12] J. J. Sakurai, *Advanced Quantum Mechanics* (Addison-Wesley, Reading, MA, 1967).

[13] K. C. Prince, M. Coreno, R. Richter, M. de Simone, V. Feyer, A. Kivimäki, A. Mihelič, and M. Žitnik, Phys. Rev. Lett. **96**, 093001 (2006).

[14] M. Coreno, K. C. Prince, R. Richter, M. de Simone, K. Bučar, and M. Žitnik, Phys. Rev. A **72**, 052512 (2005).

[15] M. Coreno, M. de Simone, M. Danailov, R. Richter, A. Kivimäki, M. Žitnik, and K. C. Prince, J. Electron Spectrosc. Relat. Phenom. **144–147**, 39 (2005).